Seasonal and Intraseasonal Modulation of Tropical Cyclogenesis Environment over the Bay of Bengal during the Extended Summer Monsoon

WATARU YANASE AND MASAKI SATOH

Atmosphere and Ocean Research Institute, The University of Tokyo, Kashiwa, Japan

HIROSHI TANIGUCHI

International Pacific Research Center, University of Hawaii at Manoa, Honolulu, Hawaii

HATSUKI FUJINAMI

Hydrospheric Atmospheric Research Center, Nagoya University, Nagoya, Japan

(Manuscript received 12 April 2011, in final form 16 September 2011)

ABSTRACT

The environmental field of tropical cyclogenesis over the Bay of Bengal is analyzed for the extended summer monsoon season (approximately May–November) using best-track and reanalysis data. Genesis potential index (GPI) is used to assess four possible environmental factors responsible for tropical cyclogenesis: lower-tropospheric absolute vorticity, vertical shear, potential intensity, and midtropospheric relative humidity. The climatological cyclogenesis is active within high GPI in the premonsoon (~May) and postmonsoon seasons (approximately October–November), which is attributed to weak vertical shear. The genesis of intense tropical cyclone is suppressed within the low GPI in the mature monsoon (approximately June–September), which is due to the strong vertical shear. In addition to the climatological seasonal transition, the authors' composite analysis based on tropical cyclogenesis identified a high GPI signal moving northward with a periodicity of approximately 30–40 days, which is associated with boreal summer intraseasonal oscillation (BSISO). In a composite analysis based on the BSISO phase, the active cyclogenesis occurs in the high GPI phase of BSISO. It is revealed that the high GPI of BSISO is attributed to high relative humidity and large absolute vorticity. Furthermore, in the mature monsoon season, when the vertical shear is climatologically strong, tropical cyclogenesis particularly favors the phase of BSISO that reduces vertical shear effectively. Thus, the combination of seasonal and intraseasonal effects is important for the tropical cyclogenesis, rather than the independent effects.

1. Introduction

The Bay of Bengal (BoB) in the north Indian Ocean (NIO) is one of the regions where tropical cyclones (TCs) form frequently (Fig. 1). Although the TC frequency over the BoB is less than those over the western and eastern North Pacific, TCs over the BoB have affected human society in the surrounding countries. For example, the Bhola cyclone caused a catastrophic death toll of 500 000 in November 1970, and tropical Cyclone Nargis took more than 130 000 victims in April–May 2008 (Webster 2008; Fritz et al. 2009).

A unique characteristic of the BoB is that TCs with maximum wind speeds exceeding 34 kt or ~17.5 m s^{-1} [referred to as tropical storms (TSs)] form in two separate seasons (black circles in Fig. 2) under the influence of the Asian summer monsoon (ASM): most of the TSs form around the premonsoon (~May) and around the postmonsoon (approximately October–November), whereas few TSs form during the mature monsoon (approximately June–September). Such a bimodal TS distribution is not observed over the other regions, where TS formation is active around summer (black circles in Fig. 13) with a unimodal distribution, except over the Arabian Sea in the NIO. On the other hand, TCs with wind speeds less than 34 kt throughout lifetimes [tropical depressions (TDs)] still form during the mature monsoon season over the BoB, which are called low pressure

Corresponding author address: Wataru Yanase, Atmosphere and Ocean Research Institute, The University of Tokyo, 5-1-5 Kashiwanoha, Kashiwa, Chiba 277-8564, Japan.
E-mail: yanase@aori.u-tokyo.ac.jp

DOI: 10.1175/JCLI-D-11-00208.1

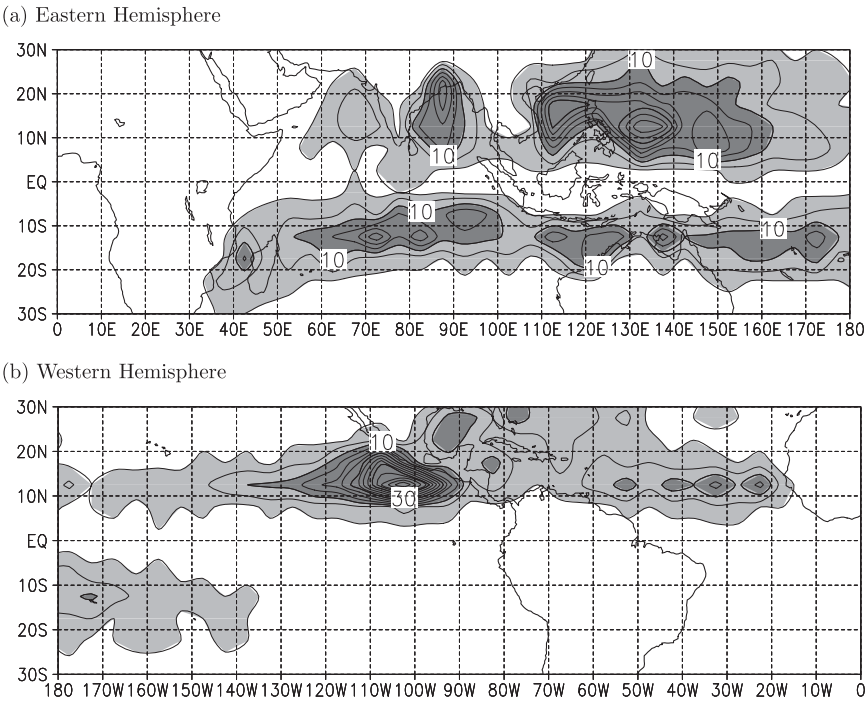

FIG. 1. Distribution of the number of tropical cyclogenesis (contour interval is five events per 5° × 5°) in 27 yr (1982–2008).

systems (LPSs; Goswami et al. 2003; Krishnamurthy and Ajayamohan 2010). These seasonal characteristics of tropical cyclogenesis (including TS and TD) over the BoB could be related to environmental conditions in the ASM region. The Bay of Bengal is a suitable region to examine the local environmental field responsible for tropical cyclogenesis, because the surrounding land on the northern, eastern, and western margins of the BoB obstructs disturbances moving from the other oceans to the BoB (Fig. 1).

Previous studies have proposed several environmental factors responsible for tropical cyclogenesis (Gray 1975; Emanuel and Nolan 2004; Camargo et al. 2007). Whereas the sea surface temperature (SST) is a well-known important factor, the activity of tropical cyclogenesis also seems to be controlled by other dynamical and thermodynamical factors including moist static stability and planetary vorticity. Emanuel and Nolan (2004) developed the genesis potential index (GPI) based on the following four factors: large lower-tropospheric absolute vorticity, weak vertical shear, high potential intensity, and high midtropospheric humidity. Weak vertical shear is necessary for tropical cyclogenesis because the shear breaks a warm core structure of TC (a ventilation effect). The potential intensity is a thermodynamical factor considering the effects of SST and moist static instability (see section 2). Camargo et al. (2007) demonstrated that the seasonal transition of GPI is in good agreement with that of tropical cyclogenesis in the major oceans including the bimodal TS season over the NIO. Another interesting characteristic of tropical cyclogenesis over the BoB or NIO is related to the boreal summer intraseasonal oscillation (BSISO). Using 30 yr of data, Kikuchi and Wang (2010) showed that the BSISO modulates the topical cyclogenesis activity over the NIO, and that the GPI is high during the active cyclogenesis phase of the BSISO. Yanase et al. (2010) proposed that the superposition of seasonal transition and BSISO caused the high GPI during the genesis of Cyclone Nargis in the premonsoon of 2008. More statistical analysis is necessary to elucidate the relation between the seasonal transition and shorter time-scale modulation that is responsible for tropical cyclogenesis over the BoB.

In the present study, we assess the statistical relation between the tropical cyclogenesis and environmental field over the BoB by addressing the following issues: 1) Are there any GPI signals on seasonal and shorter time scales in a composite analysis based on cyclogenesis events? 2) What is the relation between the seasonal transition and the shorter time-scale modulation for the cyclogenesis? 3) Which factor contributes to the modulation of GPI? These characteristics over the BoB are compared with those over the other oceans including the Arabian Sea and the North Pacific. The remainder of the manuscript is organized as follows. Section 2 describes the methodology employed in the data analysis. Section 3

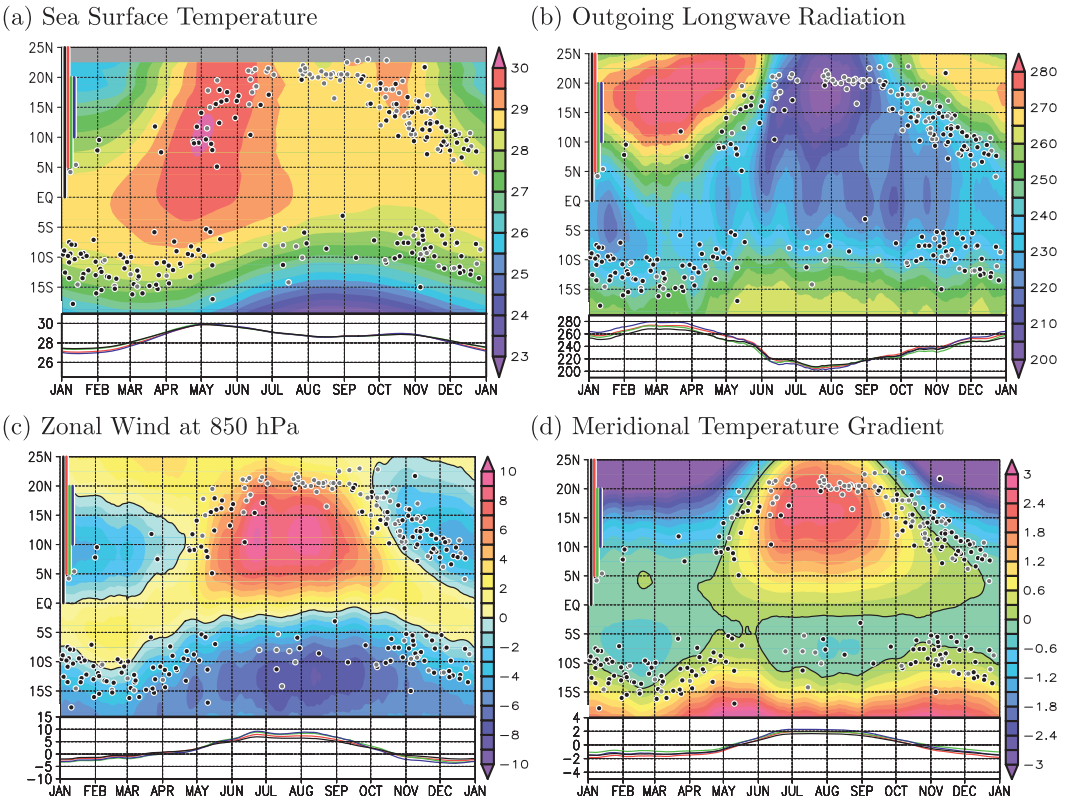

FIG. 2. Time–latitude diagram of climatological variables averaged over the BoB (80°–100°E): (a) SST (°C), (b) OLR (W m^{-2}), (c) zonal wind at 850 hPa (m s^{-1}), and (d) MTG (10^{-6} K m^{-1}). Black, red, green, and blue curves at the bottom of the panels show the averages in 0°–25°N, 5°–25°N, 5°–20°N, and 10°–20°N, respectively (the meridional ranges are shown by the lines with the same color at the top left of the panels). Black (gray) circles indicate the time and latitude of TS (TD) genesis.

presents the climatological relation between the seasonal transition of environmental field and tropical cyclogenesis. This section confirms the results of previous studies. Section 4 provides a composite analysis based on the tropical cyclogenesis to identify environmental modulations that have shorter time scales than the seasonal transition. Because the dominant shorter time-scale modulation was revealed to be the BSISO, section 5 analyzed the cyclogenesis and GPI based on the phases of the BSISO. We extended the result of Kikuchi and Wang (2010) to identify the main environmental factors that modulate the GPI within the BSISO. Section 6 discusses the cyclogenesis over the other oceans and the role of BSISO. Finally, section 7 summarizes the characteristics of the environmental field responsible for the cyclogenesis over the BoB.

2. Methodology

a. Data

The large-scale environmental field analyzed in this study comprises daily data on the atmosphere and ocean between 1982 and 2008. Atmospheric analysis data are the Japanese 25-yr Reanalysis (JRA-25) for the period between 1979 and 2004 (Onogi et al. 2007) and the Japan Meteorological Agency (JMA) Climate Data Assimilation System (JCDAS) for the period from 2005, which are provided by the JMA and the Central Research Instituted of Electric Power Industry (CRIEPI); because JCDAS is based on the same system as that employed by JRA-25, the two products, when combined, provide a homogeneous dataset for the period from 1979 to 2008. The horizontal resolutions of the products are 1.25° grid intervals. The original 6-hourly dataset of JRA-25/JCDAS is averaged every four time steps to create a daily dataset. Convective activity is represented by outgoing longwave radiation (OLR) of the National Oceanic and Atmospheric Administration (NOAA). The analysis data of SST is the product of NOAA Optimum Interpolation from late 1981, which uses in situ and satellite data (Reynolds et al. 2002). The original weekly dataset of SST, with a horizontal resolution of 1°, is linearly interpolated in time and space to create a daily dataset on the same grid system as that used in the atmospheric dataset.

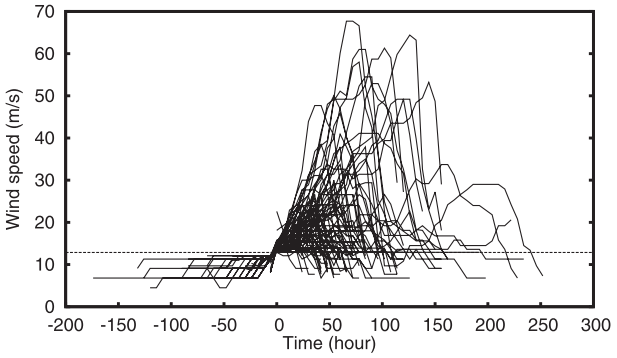

FIG. 3. Wind speeds of tropical cyclones over the BoB relative to the cyclogenesis (0 h). Dashed line indicates the wind speed of ~12.9 m s^{-1} (25 kt).

In any analysis of the environmental field of topical cyclogenesis, it is important that the temporal and spatial scales of environmental modulation are larger than those of TC itself because the TC influences the atmospheric and oceanic fields transiently. To avoid this problem, TC-scale fields are removed by the spatial filter of Kurihara et al. (1993); the parameter of the spatial filter is set to remove the wavelength shorter than 8.75° in this study. In addition, a 15-day running mean is used to filter out the TC-scale signal in the time direction. Herein, this spatially and temporally filtered data is referred to as an environmental field.

Information regarding the locations and intensities of individual TCs for the period 1982–2008 is derived from a best-track dataset obtained from the International Best Track Archive for Climate Stewardship (IBTrACS; Knapp et al. 2010). Here, a tropical cyclogenesis is defined as the time when the surface wind speed first exceeded the threshold of 12.9 m s^{-1} (25 kt) in the lifetime. This definition includes TSs and intense TDs. Intense TDs are analyzed to obtain supplementary samples (gray circles in Fig. 2) in the mature monsoon season when few TSs are observed over the Bay of Bengal. Figure 3 shows time series of surface wind speed of TCs over the BoB analyzed in the present study, and Table 1 summarizes the monthly number of TCs observed over the Bay of Bengal between 1982 and 2008.

b. Genesis potential index

The environmental field responsible for tropical cyclogenesis is assessed by the GPI proposed by Emanuel and Nolan (2004), which is defined based on four environmental factors:

$$\mathrm{GPI} = |10^5\eta|^{3/2}(1 + 0.1V_{\mathrm{shear}})^{-2}\left(\frac{V_{\mathrm{pot}}}{70}\right)^3\left(\frac{H}{50}\right)^3,$$

TABLE 1. Monthly cyclogenesiss number for TDs and TSs over the BoB between 1982 and 2008.

Month	1	2	3	4	5	6	7	8	9	10	11	12
TD	2	0	0	0	4	9	6	13	8	16	5	5
TS	2	1	2	4	13	5	1	0	3	17	23	8

where η is the absolute vorticity at 850 hPa (s^{-1}), V_{shear} is the magnitude of the vertical wind shear between 850 and 200 hPa (m s^{-1}), V_{pot} is the potential intensity (m s^{-1}), and H is the relative humidity at 600 hPa (%). The potential intensity V_{pot} considers SST and vertical profiles of temperature and specific humidity in the troposphere, and is defined as

$$V_{\mathrm{pot}}^2 = \frac{T_s}{T_0}\frac{C_k}{C_D}(\mathrm{CAPE}^* - \mathrm{CAPE}^b),$$

where T_S is SST, T_0 is the mean outflow temperature at the level of neutral buoyancy, C_k is the exchange coefficient for enthalpy, C_D is the drag coefficient, CAPE* is the convective available potential energy (CAPE) for an air parcel at the radius of maximum winds, and CAPE^b is the CAPE for an air parcel lifted from the lowest data grid (1000 hPa) in the ambient atmosphere (Bister and Emanuel 2002; Camargo et al. 2007).

3. Climatological seasonal transition

The seasonal transition seems to be the most dominant environmental modulation responsible for tropical cyclogenesis. Figure 2 shows time–latitude diagrams of basic variables averaged over the BoB (80°–100°E). The SST over the Bay of Bengal shows a bimodal annual distribution with the peaks in the pre- and postmonsoon seasons (shadings and curves in Fig. 2a), which is unique to the BoB and the Arabian Sea in the NIO. Although the bimodal annual distribution of SST is qualitatively similar to that of TS genesis, the SST alone cannot explain the following characteristics: the TS genesis is most active in the postmonsoon, whereas the SST is highest in the premonsoon; and the SST exceeding 28.5°C in the mature monsoon season is enough high for TS genesis. The most active convection over the BoB (the lowest OLR in Fig. 2b) occurs in the mature monsoon season, when the TS genesis over the BoB is reduced. Note that the numbers of tropical cyclogenesis over the North Pacific and the North Atlantic are increased during summer characterized by the active convection (not shown). Over the BoB, a monsoon flow represented by the zonal wind changes the sign in the pre- and postmonsoon seasons (Fig. 2c). Apparently, most of the TS genesis occurred during these transitions of the monsoon flow. Meridional

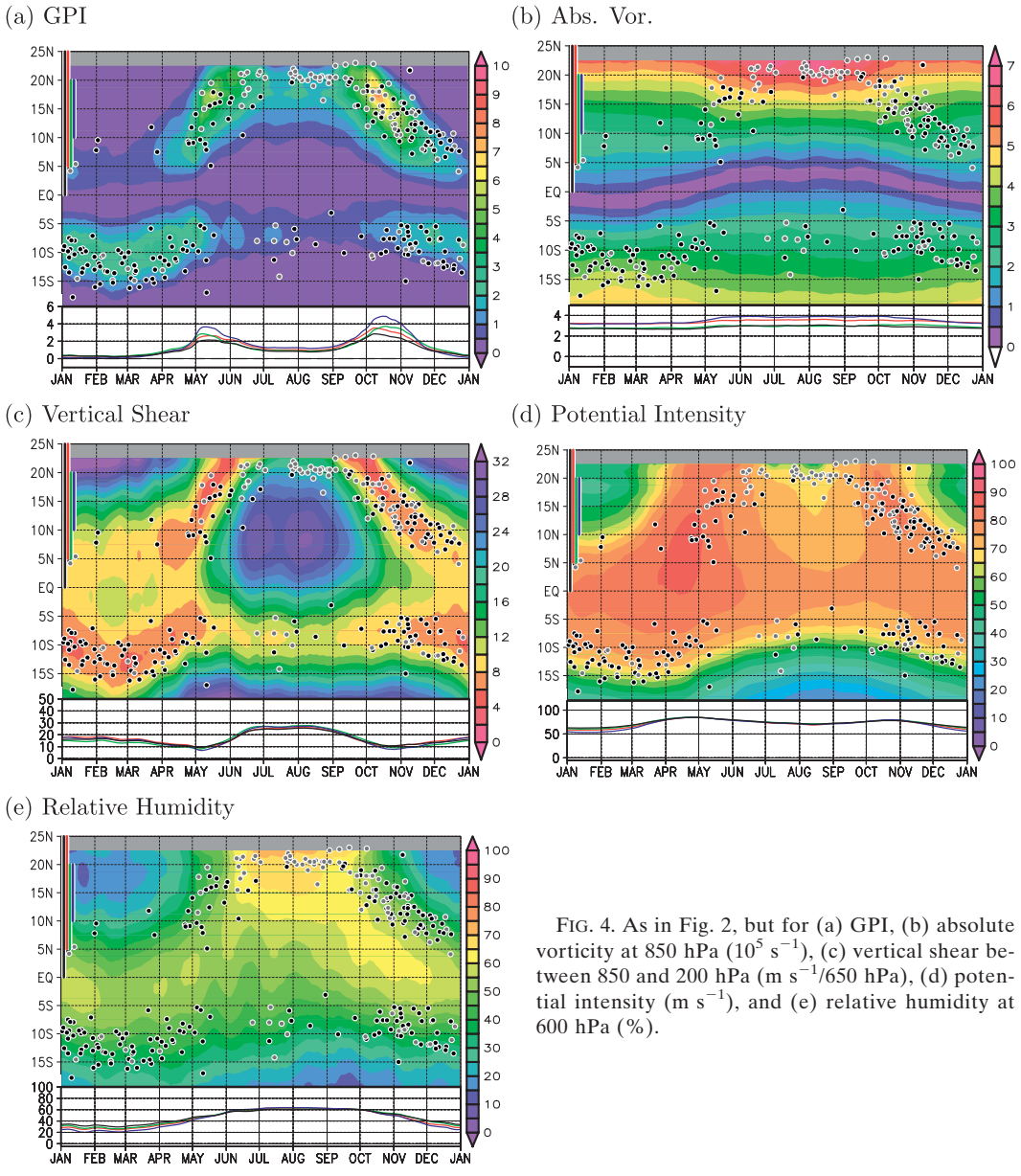

FIG. 4. As in Fig. 2, but for (a) GPI, (b) absolute vorticity at 850 hPa (10^5 s^{-1}), (c) vertical shear between 850 and 200 hPa (m s^{-1}/650 hPa), (d) potential intensity (m s^{-1}), and (e) relative humidity at 600 hPa (%).

temperature gradient (MTG) in the upper troposphere (200–500 hPa) is another index of the ASM (Mao and Wu 2007). In general, the MTG is negative in the Northern Hemisphere because of the meridional difference of solar radiation. However, the MTG during the mature ASM is uniquely positive, which is attributed to the heating of the Asian continent to the north of the BoB. Thus, the MTG changes the sign in the pre- and postmonsoon seasons (Fig. 2d), when most of the TS formations are observed.

To understand why the pre- and postmonsoon seasons are favorable for TS genesis, GPI and its four factors are analyzed (Fig. 4). GPI shows bimodal annual distribution (Fig. 4a) with the peaks in the pre- and postmonsoon, which is in good agreement with the TS activity over the BoB. This is consistent with the result of Camargo et al. (2007). The GPI is moderate during the mature monsoon, when only TDs form. In addition, GPI qualitatively explains the meridional distribution of TS genesis, including a northward shift in the premonsoon and a southward shift in the postmonsoon. Note that TS genesis in the Southern Hemisphere also occurs during the high GPI seasons from October to May.

The four GPI factors give further information on the environment responsible for the bimodal TS genesis. The bimodal GPI distribution is dominantly attributed to weak vertical shear in the pre- and postmonsoon

(shadings and curves in Fig. 4c). In the mature monsoon season, strong vertical shear seems to prevent TCs from developing to TS intensity by the ventilation effect. Based on the thermal wind balance, the weak vertical shear is associated with the small MTG in the pre- and postmonsoon over the BoB (Fig. 2d). The potential intensity also shows a weak bimodal distribution (Fig. 4d), which reflects the SST distribution (Fig. 2a). The seasonal transition of absolute vorticity is relatively weak (Fig. 4b) because of the large planetary vorticity. Midtropospheric relative humidity is highest during the mature monsoon (Fig. 4e), which is related to the active convection as shown in Fig. 2b. In summary, the bimodal annual distribution of climatological GPI is attributed to the weak vertical shear dominantly and to the high potential intensity secondarily.

4. TC-based composite analysis

The seasonal transition of climatological GPI in section 3 is in good agreement with the tropical cyclogenesis: TS genesis occurs within the high GPI environment in the pre- and postmonsoon seasons, whereas only TD forms within the moderate GPI environment in the mature monsoon. If the large-scale environment modulates on a time scale shorter than the seasonal transition, it is of interest to examine whether GPI can explain the cyclogenesis even on such a short time scale statistically. To extract signals of environmental modulation, we attempt a composite analysis based on the cyclogenesis events (TC-based composite analysis).

As the climatological seasonal transition is the large environmental modulation, the original field (total field) is separated into climatological and anomalous ones in advance of the composite analysis: the climatological field is the average of 27 yr, whereas the anomalous field is the difference between the total and the climatological ones. Then the TC-based composite is performed for the total, climatological, and anomalous fields. As the cyclogenesis activity is different between seasons (Fig. 4), the composite field is assessed for three seasons: April–May (AM; premonsoon over the BoB), June–September (JJAS; mature monsoon) and October–November (ON; postmonsoon). To obtain the time evolution of environmental modulation, the composite is performed for the period from 30 days before the cyclogenesis (−30 relative day) to 30 days after the cyclogenesis (30 relative day). It should be noted again that the analysis is performed using the environmental fields (spatially and temporally filtered data).

Figure 5 shows time–latitude diagrams of the TC-based composite GPI. Here, the relative day 0 is the time when the cyclogenesis events occur, and the short horizontal bars indicate the latitude of cyclogenesis. In the premonsoon (the left column in Fig. 5), a high GPI signal in the total field shifts northward from 5° to 20°N during the period between −20 and 10 days (Fig. 5a). This northward-moving signal is attributed to both the climatological and anomalous modulations. In the climatological field (Fig. 5d), a high GPI signal slowly shifted northward during the period from −30 to 30 days, which is the seasonal transition observed in Fig. 4a. In the anomalous field (Fig. 5g), a positive GPI signal moves northward quickly from −20 to 10 days, which is enough intense to modify the climatological field. Most of the cyclogenesis in the premonsoon occurs within the positive anomaly of the northward-moving GPI signal. The positive GPI anomaly is followed by a negative one, and then by a weak positive one again, showing a periodicity of approximately 30–40 days. For the mature monsoon (the middle column in Fig. 5), a high GPI signal in the climatological field is stationary around approximately 15°–20°N. In the anomalous field, on the other hand, a high GPI signal moves fast northward as observed in the premonsoon season. In the postmonsoon season (the right column in Fig. 5), a high GPI signal in the climatological field slowly shifts southward, which is the seasonal transition shown in Fig. 4a. In the anomalous field, a high GPI signal still moves northward. Thus, the northward-moving anomaly with the intraseasonal time scale (approximately 30–40 days) is observed in all the analyzed seasons, although it is a little obscure in the postmonsoon season.

The northward-moving signal in the anomalous field is simply observed in the time–latitude diagram of zonal wind at 850-hPa pressure level (Fig. 6). In the climatological field, the westerly flow over the BoB increases in the premonsoon, remains almost static in the mature monsoon, and then decreases in the postmonsoon (Figs. 6d–f). The anomalous fields of zonal wind show fast northward-moving signals in all the seasons again (Figs. 6g–i): a westerly anomaly to the south of the cyclogenesis and an easterly one to the north. In the longitude–time diagrams of the composite field (not shown) the signal almost remain static, and shows the zonal scale of 40° or more. Because the signal has the large horizontal scale and long time scale, it is not merely the influence of TC itself.

To elucidate the environmental modulation responsible for the high GPI, the four GPI factors are assessed using the TC-based composite analysis. Figure 7 shows time–latitude diagrams of the anomalous fields of the four factors in the three seasons. The absolute vorticity (Figs. 7a–c) shows a positive signal quickly moving northward in all the seasons. As planetary vorticity does not change in time, the northward-moving signal is

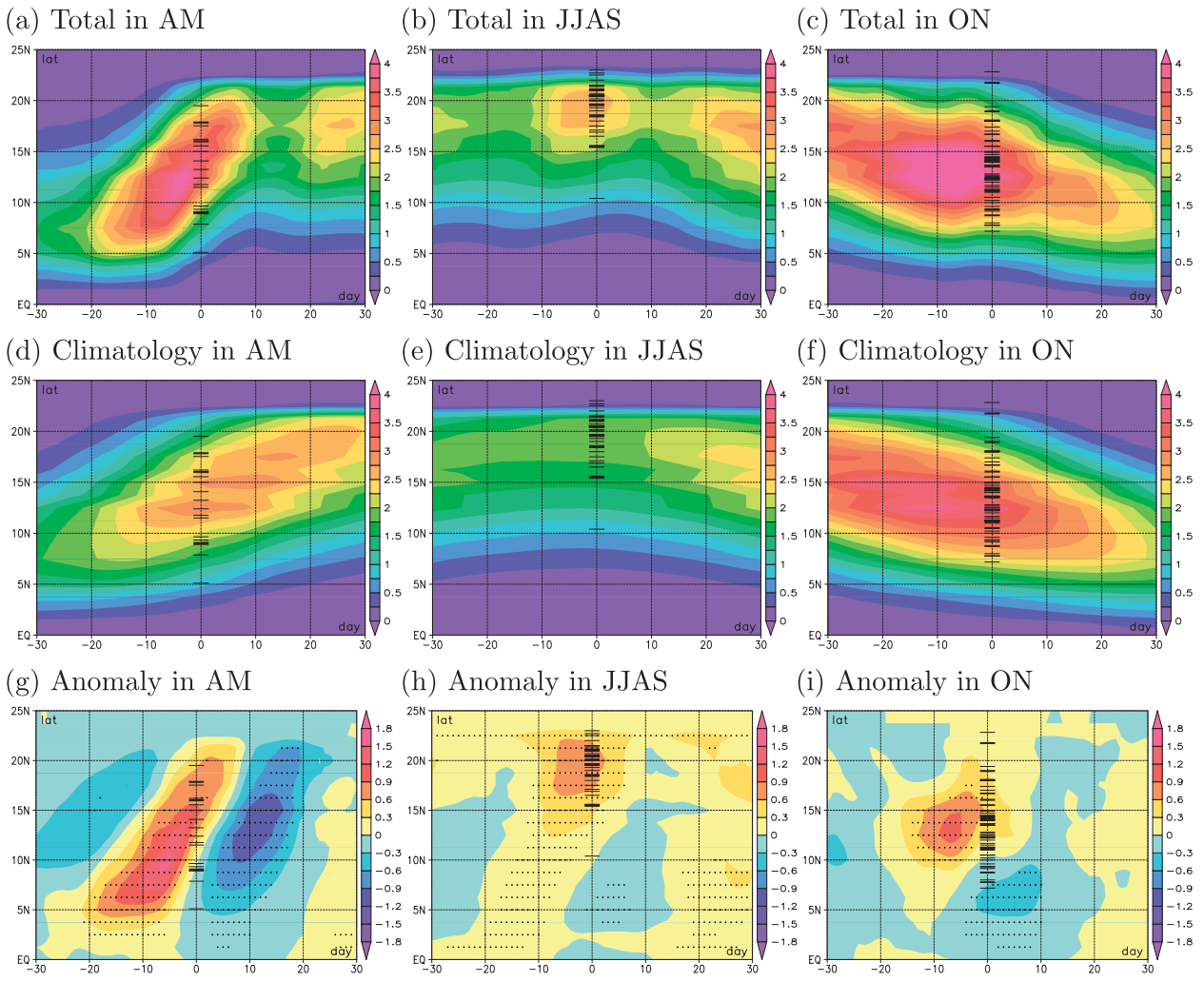

FIG. 5. Time–latitude diagram of GPI over the BoB in the TC-based composite analysis. Diagrams for months of (left) AM, (middle) JJAS, and (right) ON. Diagrams for (top) total, (middle) climatological, and (bottom) anomalous fields. Dotted areas correspond to differences in the anomaly at $p < 0.1$ using Student's t test. Short horizontal bars at day 0 indicate the latitudes of individual cyclogenesis.

caused by the change in relative vorticity, which is large on the northern (southern) side of the westerly (easterly) axes in Figs. 6g–i. Most of the cyclogeneses occur around the positive anomaly of absolute vorticity. In detail, the cyclogeneses in the mature monsoon prefer the northern side of the axis of the positive anomaly—that is, the cyclogeneses in the mature monsoon occur farther north than those in the pre- and postmonsoon relative to the northward-moving signal, which is discussed in section 6. The vertical shear (Figs. 7d–f) also shows the northward-moving signal particularly in the pre- and mature monsoon seasons. The cyclogenesis in the mature monsoon prefers the region of weak vertical shear (Fig. 7e), whereas the cyclogenesis in the pre- and postmonsoon is observed both in positive and negative anomalies (Figs. 7d,f). The potential intensity (Figs. 7g–i) does not show the oscillation of approximately 30–40 days, although some longer-period signal is observed in the premonsoon (Fig. 7g). Similar to the absolute vorticity, the cyclogenesis occurs within the positive anomaly of relative humidity (Figs. 7j–l), and tends to occur on the northern side of the axis of positive anomaly in the mature monsoon.

In summary, the tropical cyclogenesis in the pre-, mature-, and postmonsoon seasons occurs within the northward-moving signal of high GPI anomaly, which had a zonal scale more than 40° and the periodicity of approximately 30–40 days. The high GPI is related to the large absolute vorticity and high relative humidity in all the seasons, whereas it is also related to the weak vertical shear in the mature monsoon. The cyclogenesis in the mature monsoon occurs farther north than those in the pre- and postmonsoon relative to the axis of northward-moving signals. The northward-moving signal

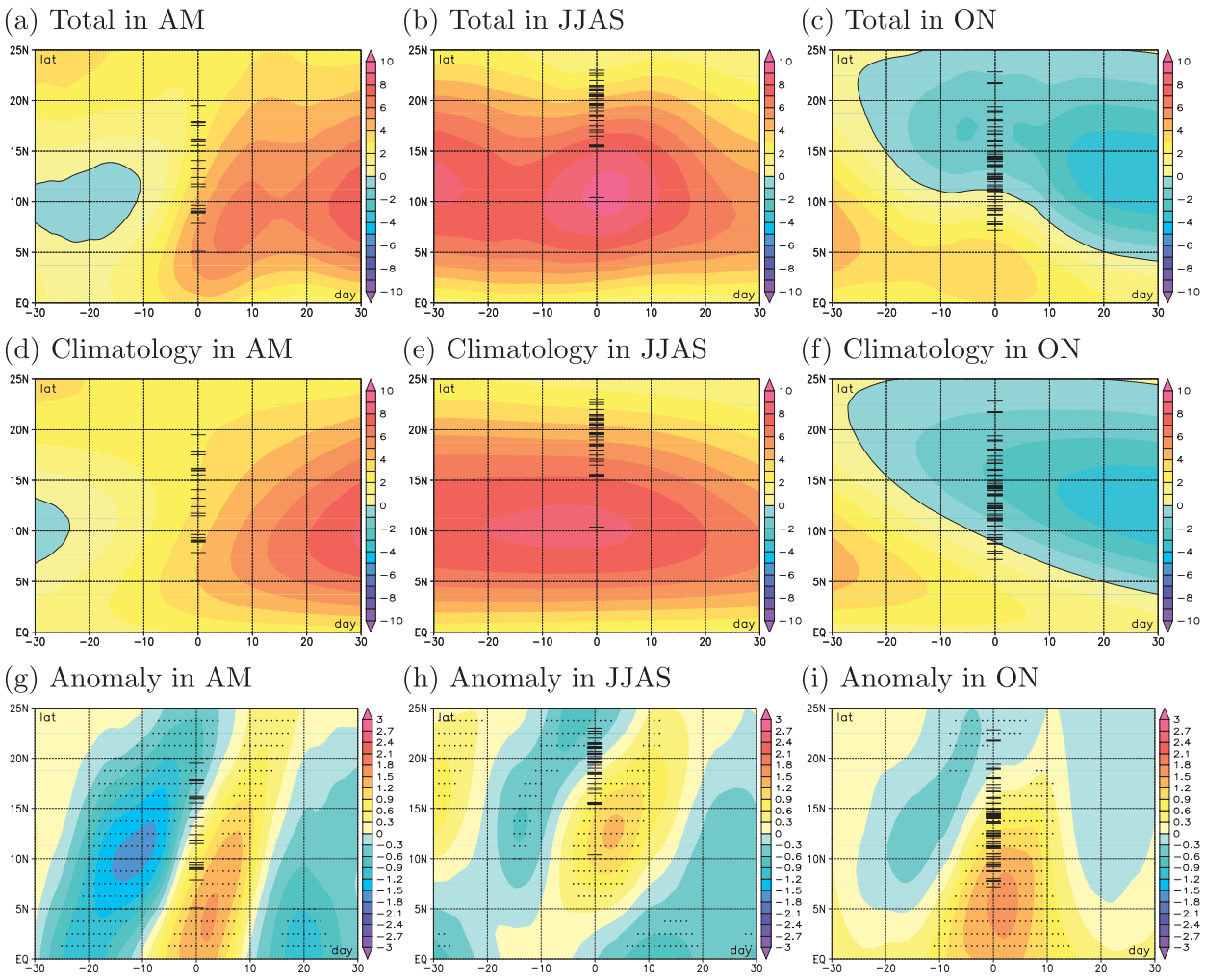

FIG. 6. As in Fig. 5 but for zonal wind at 850 hPa.

of high GPI is more significant in the pre- and mature monsoon seasons than in the postmonsoon season. The TC-based composite is also useful to assess whether the environmental modulation is the cause or effect of the tropical cyclogenesis; given that the signal of GPI appears 20 days prior to the cyclogenesis, reaching its maximum before the genesis, the signals are not merely the response of the cyclogenesis. As the signal is accompanied by the modulation of zonal flow and relative humidity, it seems to be associated with the BSISO (Jiang et al. 2004). In the next section, the relation between the cyclogenesis and the BSISO is analyzed.

5. BSISO-based composite analysis

The TC-based composite analysis in section 4 clarified that the most dominant signal in the anomaly field appears to be relevant to the BSISO. This section focuses on the environmental modulation responsible for tropical cyclogenesis in terms of the phase of the BSISO. Based on the previous studies (Yasunari 1981; Murakami et al. 1984; Goswami and Mohan 2001), the BSISO is defined by 30–60-day filtered zonal wind at 850 hPa. Here, the cyclogenesis from May to October is assessed, given that the amplitude of the BSISO mode is large during this period (Kikuchi and Wang 2010). Note that the positive MTG over the BoB during this period (the curves in Fig. 2d) corresponds to the ASM season. To minimize the influence of the TC itself on the BSISO signal, the zonal wind is averaged in the large area (10°–20°N and 60°–110°E; the rectangle in Fig. 9), which is determined based on the structure of the BSISO shown in the previous studies (Murakami and Nakazawa 1985; Goswami and Mohan 2001). Figure 8a shows the time series of the BSISO index in 2008. Each minimum–maximum–minimum cycle is divided into eight phases in the following

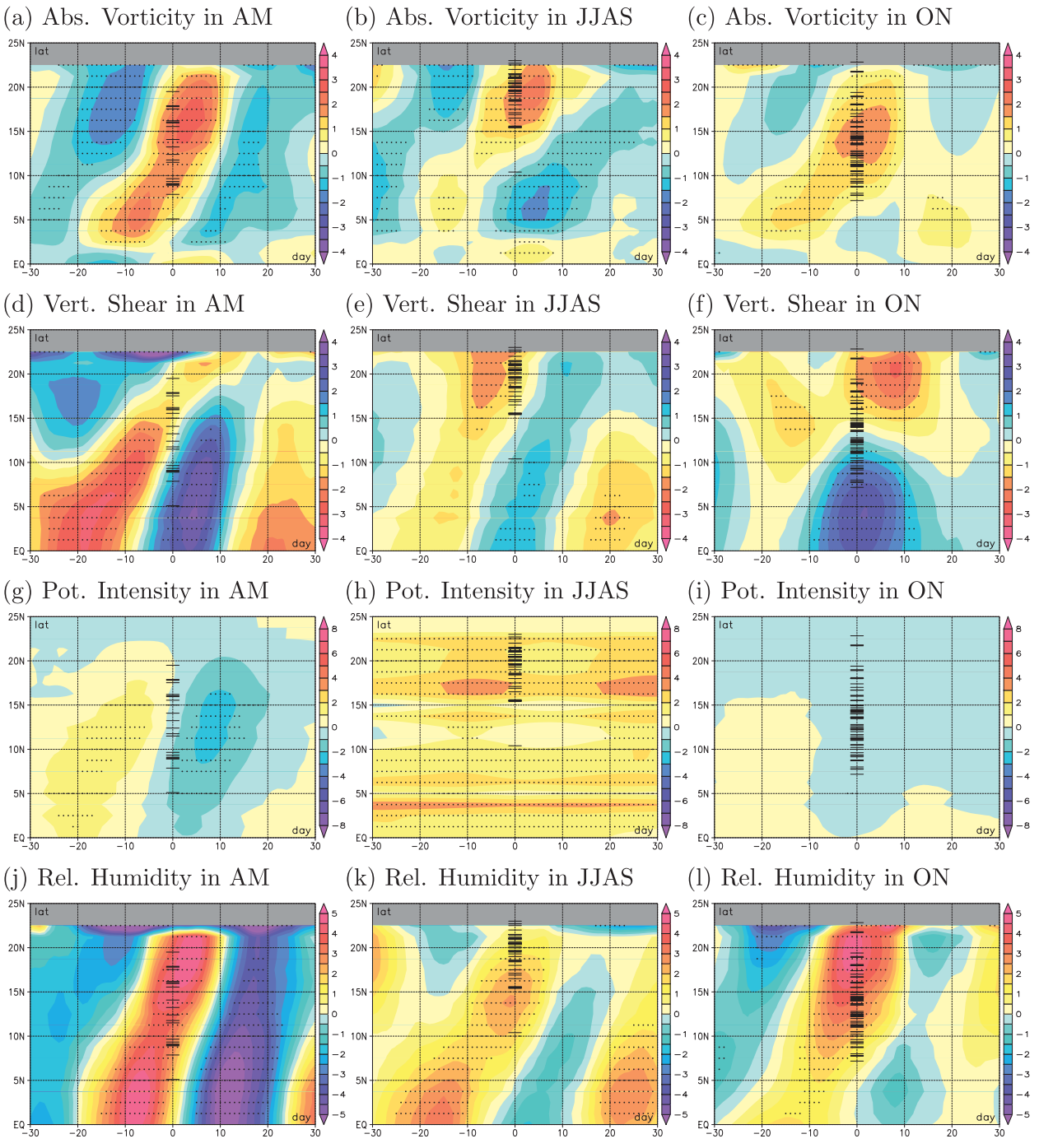

FIG. 7. As in Figs. 5g,h,i but for the anomalous fields of (a)–(c) absolute vorticity at 850 hPa (10^{-5} s^{-1}), (d)–(f) vertical shear [m s^{-1}(650 hPa)$^{-1}$], (g)–(i) potential intensity (m s^{-1}), and (j)–(l) relative humidity at 600 hPa (%).

manner (Fig. 8b): phases 1–4 (5–8) are defined by separating the period between the first minimum and the maximum (between the maximum to the next minimum) evenly. If the amplitude of the signal (the half of the difference between a maximum and a minimum) is less than one standard deviation, the period is not analyzed because of the weak BSISO. Composite of the environmental fields (spatially and temporally filtered data as described in section 2) and count of cyclogenesis are performed for each phase of the BSISO.

Figure 9 shows composite patterns of zonal wind at 850 hPa and OLR for phases 1, 3, 5, and 7. In phase 1,

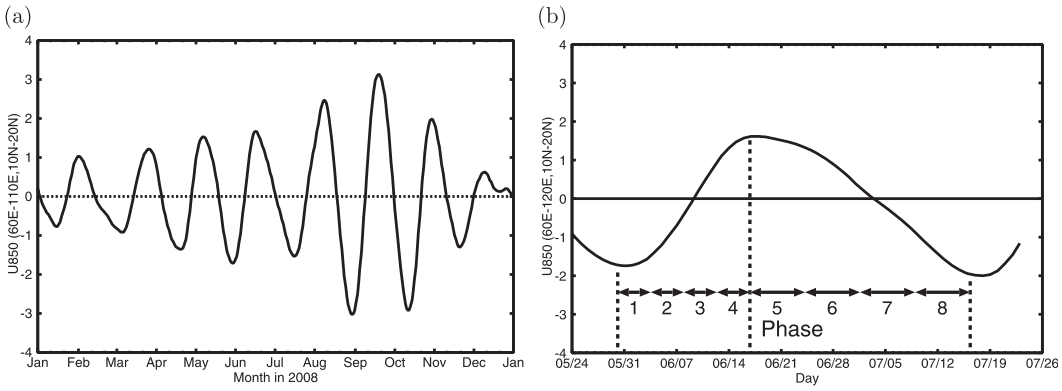

FIG. 8. Time series of 30–60-day bandpath-filtered zonal wind at 850 hPa averaged in the region (10°–20°N, 60°–110°E). (a) Time series in 2008. (b) Definition of eight phases of the BSISO.

a westerly anomaly is observed near the equator over the Indian Ocean, and active convection (negative OLR) occurs to the north of the westerly axis. From phases 1 to 5, the westerly axis and active convection shift northward from the equator to the BoB. In phase 7, the westerly axis almost disappears over the Indian Ocean, which is the end of a BSISO cycle.

Figure 10a shows the number of tropical cyclogeneses for each phase. The cyclogenesis is significantly modulated by the phase of the BSISO: the number of cyclogeneses in phases 3 and 4 are 20 and 23, respectively, whereas those in phases 1 and 8 are only 2. Phases 3 and 4 are characterized by active convection over the BoB (Fig. 9b). This is consistent with the result of Kikuchi and Wang (2010) using an extended empirical orthogonal function (EEOF) for the BSISO definition. As the numbers of analyzed days are not much different between the phases (approximately 392–467 days; Fig. 10b), the difference in cyclogenesis numbers between the phases is attributed to the BSISO dynamics. For the weak BSISO period, the number of cyclogenesis is 21 for 1638 analyzed days. This frequency (0.013 events per day) is nearly the same as those for phases 5–7.

The phase–latitude diagrams of GPI and its four factors in the BSISO-based composite analysis are shown in Fig. 11 together with the months of the cyclogenesis (digits in the figure). The total GPI is largest from phases 2 to 4 between 15° and 20°N, where the cyclogenesis is active (Fig. 11a). The anomalous field of GPI shows a positive signal moving northward from phases 1 to 4 (Fig. 11a). The cyclogenesis is active around the positive region of GPI anomaly, although the timing seems to be delayed by ~1 phase. This lag may indicate the time during which a TC grows gradually. To assess the individual contributions of the four GPI factors quantitatively, the GPI is recalculated using the climatological fields (1982–2008) of three out of the four factors, but using the unmodified daily fields of the target factor (cf. Camargo et al. 2009). Figures 11c–f show the contribution of the four factors to the GPI anomaly. The relative humidity dominantly contributes to the high GPI. The absolute vorticity changes in a similar manner to the relative humidity, although the contribution is relatively small. The GPI anomaly caused by vertical shear is accompanied more by the cyclogenesis from June to September than by those in May and October (Fig. 11d), which is consistent with the result of TC-based composite analysis (Fig. 7e).

As the sign of GPI anomaly in a BSISO phase also changes in the meridional direction, the analysis is more effective if the BSISO phase is adjusted based on the latitude. Therefore, all the cyclogeneses are moved to the latitude of 20°N (the dashed line in Fig. 11) along the line parallel to the northward movement of the BSISO signal (the solid line in Fig. 11). Figure 12 shows the cyclogenesis number recalculated in the latitude-adjusted BSISO phases. The cyclogenesis distribution with the peak around phase 4 in the adjusted phase is more symmetric than that in the original BSISO phase (Fig. 10a). The ratio of cyclogenesis from June to September (gray bars) is high between phases 2 and 4, whereas those in May and October (black and white bars, respectively) are high between phases 4 and 7. This indicates that the cyclogenesis in the mature monsoon occur in an earlier phase (or farther north relative to the BSISO phase) than those in the pre- and postmonsoon. Thus, the cyclogenesis in the mature monsoon prefers the BSISO phase that reduces the vertical shear effectively.

6. Discussion

a. Comparison with other oceans

The previous sections described the seasonal and intraseasonal characteristics of the environmental field

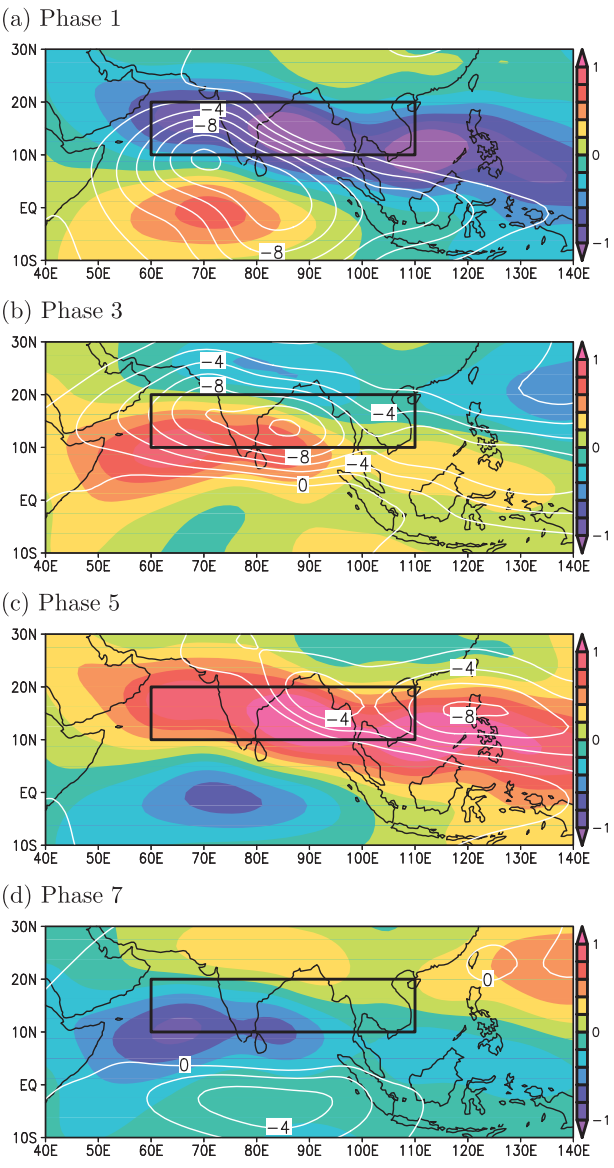

FIG. 9. Composite of zonal wind anomaly at 850 hPa (shading) and negative OLR anomaly (white contours with contour interval of 2 W m^{-2}) for phases (a) 1, (b) 3, (c) 5, and (d) 7 of the BSISO. The black rectangle shows the region in which the zonal wind is averaged for making the BSISO index.

responsible for tropical cyclogenesis over the BoB. To understand whether such characteristics are unique to the BoB, cyclogenesis over the following oceans are examined: the Arabian Sea in the NIO (55°–75°E), the western North Pacific (125°–145°E), the eastern North Pacific (95°–115°W), and the North Atlantic (30°–50°W). The above regions of 20° in longitude cover the most active cyclogenesis region (Fig. 1).

To compare the seasonal transitions, time–latitude diagrams of the climatological GPI field for the four regions are shown in Fig. 13 (see also Fig. 4a for the BoB). The tropical cyclogenesis and high GPI over the Arabian Sea show bimodal annual distribution (Fig. 13a), which is similar to those over the BoB, whereas those over the other regions are characterized by unimodal distribution from boreal summer to autumn (Figs. 13b–d). Therefore, the bimodal distribution of cyclogenesis and high GPI is unique to the NIO including the BoB and the Arabian Sea, which is consistent with the previous studies (Camargo et al. 2007; Kikuchi and Wang 2010; Evan and Camargo 2011). The high GPI in the pre- and post-monsoon over the Arabian Sea is associated with the weak vertical shear and high potential intensity (not shown), which is also the same characteristics as the BoB. The other region shows weak vertical shear and high potential intensity in summer (not shown). The strong vertical shear over the NIO in summer is related to the large positive MTG in the ASM region through the thermal wind balance. Therefore, the heating of the Asian continent to the north of the NIO during the summer is responsible for the bimodal annual distribution of TSs over the NIO.

The intraseasonal characteristics over the NIO are also different from those over the other oceans. Figure 14 shows the time–latitude diagram of the anomalous GPI field for the four oceans in the TC-based composite analysis (see also the bottom row in Fig. 5 for the BoB). Here, the tropical cyclogenesis used in the composite analysis over the western and eastern North Pacific and North Atlantic is limited to the cases between 10° and 20°N, as the composite analysis would be obscure if cyclogenesis locations are diverse. In the JJAS season, the anomalous GPI field over the Arabian Sea shows a northward-moving signal, whereas those over the other oceans are weak or nearly stationary. The northward-moving signal over the Arabian Sea is associated with the BSISO in the ASM because the zonal scale of the signal extends over the entire NIO (see Fig. 9). In the AM season, the northward signal is also observed over the western and eastern North Pacific as well as the Arabian Sea. Because the signal over the western North Pacific is also accompanied by significant eastward movement in the longitude–time diagram (not shown), it seems to be related to the MJO (Madden and Julian 1972). On the other hand, the signal over the eastern North Pacific is almost stationary in the zonal direction (not shown), which should be studied in a future work. Thus, the BoB and the Arabian Sea in the NIO have similar dynamics for tropical cyclogenesis both on the seasonal and intraseasonal time scales, although more samples over the Arabian Sea may be necessary to make a more reliable conclusion.

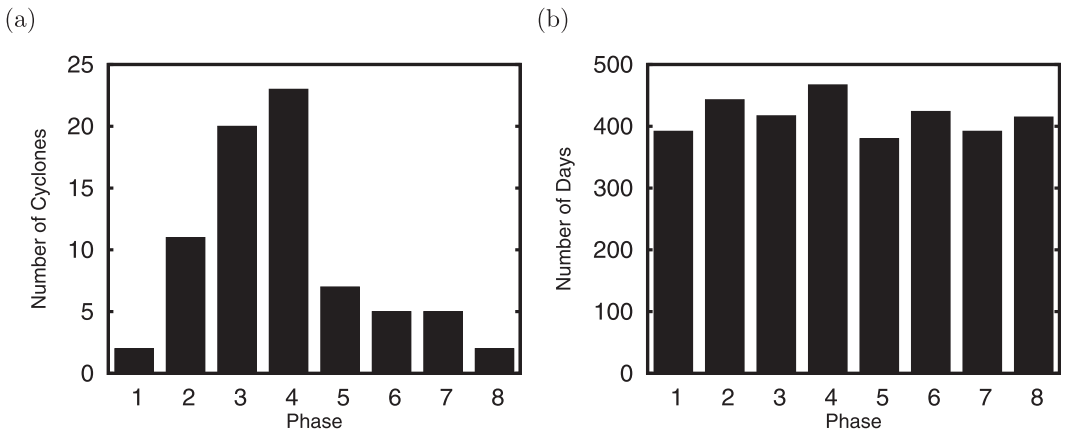

FIG. 10. Numbers of the events in each phase of the BSISO. (a) Tropical cyclogenesis. (b) Total observed day.

b. *Dynamical relation between tropical cyclogenesis and BSISO*

The TC-based composite analysis showed that the northward-moving signal of high GPI is attributed to the large relative vorticity, high relative humidity, and weak vertical shear (Figs. 5 and 7). These characteristics are consistent with the structure and dynamics of the BSISO (Jiang et al. 2004): the lower-tropospheric vorticity causes active convection through the convergence in the Ekman layer, whereas the convection intensifies the lower-tropospheric vorticity through the stretching effect of vortex. This results in the good correlation between the lower-tropospheric vorticity and midtropospheric humidity. The structure of the vertical shear in the BSISO results from the superposition of the BSISO flow and climatological one: because the lower-tropospheric positive vorticity in the BSISO is accompanied by the easterly (westerly) to the north (south), the vertical shear of the zonal flow is westerly (easterly) to the north (south). Given the climatological easterly vertical shear over the Bay of Bengal during the ASM season, the magnitude of the total vertical shear of zonal flow is weak (strong) to the north (south) of the lower-tropospheric positive vorticity. The modulation of vertical shear by the BSISO works more effectively in the mature monsoon (Fig. 11d), presumably because the very strong vertical shear in the climatological field plays a key role to inhibit the cyclogenesis (Fig. 4c). It is also speculated that the BSISO modulation may not give sufficient time for TDs in the mature monsoon to develop to the TS intensity.

The present study has demonstrated that the active tropical cyclogenesis occurs within the high GPI caused by the BSISO. However, other dynamics might explain the relation between the cyclogenesis and the BSISO. Krishnamurti et al. (1981) proposed that barotropic instability might promote the cyclogenesis over the Arabian Sea during the onset of ASM. They analyzed the meridional gradient of the absolute vorticity (MGAV) using the zonally averaged westerly wind at 850 hPa, as the necessary condition for the existence of barotropic instability is MGAV vanishing somewhere on the meridional plane. They demonstrated that the zero line of MGAV was observed during the period of cyclogenesis in June 1979. To examine the barotropic instability over the Arabian Sea and the BoB, TC-based composite of MGAV is analyzed for both oceans. Figure 15 shows the total field of the MGAV over the Arabian Sea and the BoB. Here, any spatial filter is not used, because the zero line of MGAV has very narrow structure in the meridional direction. Over the Arabian Sea, the MGAV in the JJAS season shows the zero line around 20°N (Fig. 15b), where most of the cyclogenesis occurs. This is consistent with the result of Krishnamurti et al. (1981). On the other hand, MGAV over the BoB shows no zero line in all the seasons (Figs. 15d–f). In detailed analysis for individual cases, the cyclogenesis around the ASM onset over the Arabian Sea occurs near the zero line of MGAV in most cases (not shown), whereas those over the BoB showed weaker relation with the zero line of MGAV. Therefore, the barotropic instability seems to work more dominantly over the Arabian Sea than over the BoB, although more careful analysis is necessary to obtain a clear conclusion.

For individual tropical cyclogenesis, finite-amplitude disturbances (seeds) may be necessary (Rotunno and Emanuel 1987), although the GPI can explain the statistical probability of cyclogenesis. As the detailed dynamics of individual cyclogenesis are not the target in the present study, the following studies only suggest several candidates for the cyclogenesis seeds over the BoB. Kikuchi and Wang (2010) proposed that a westerly wind burst in the BSISO can provide a synoptic-scale

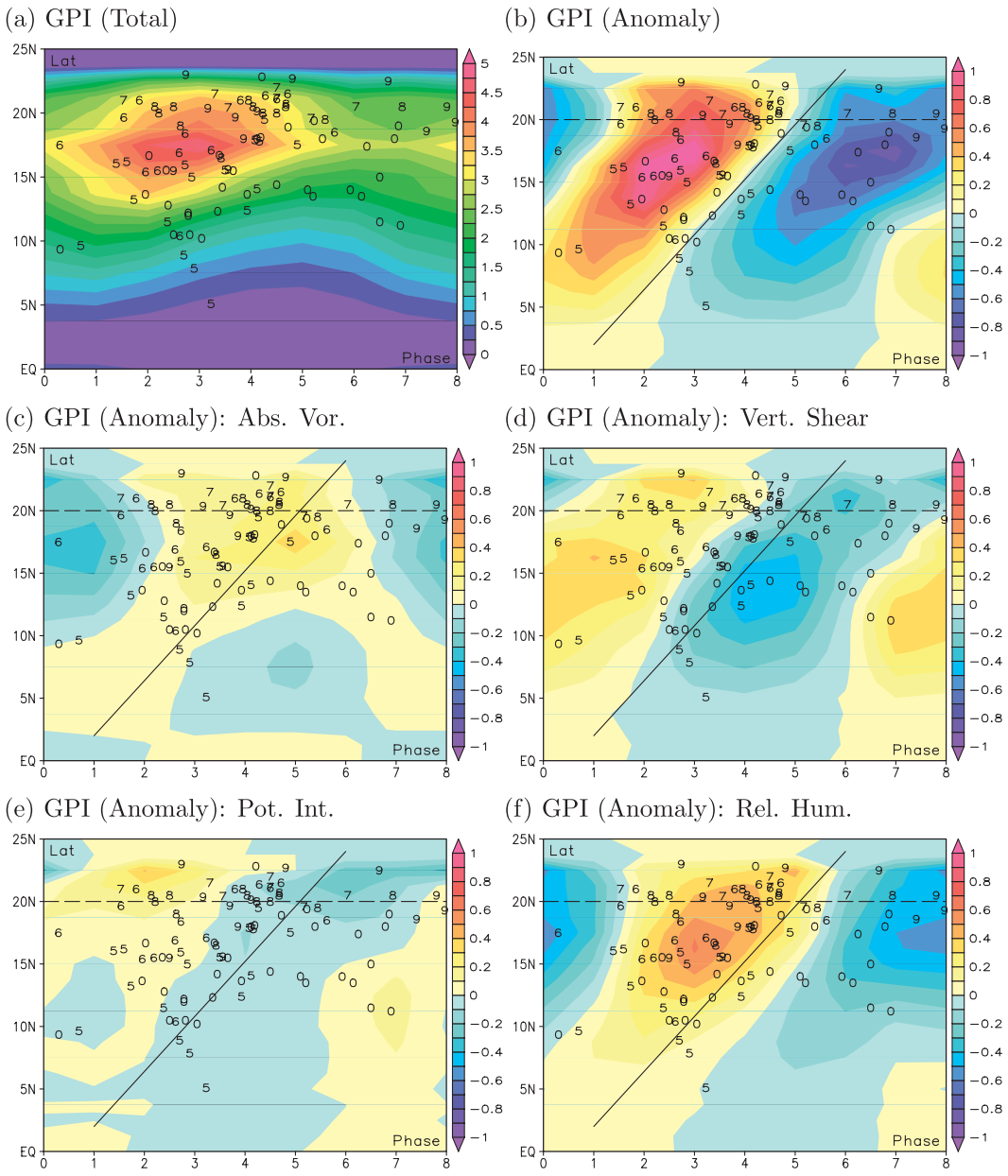

FIG. 11. Phase–latitude diagram obtained by the BSISO-based composite analysis: (a) GPI (total), (b) GPI (anomaly), (c) contribution of absolute vorticity to GPI (anomaly), (d) contribution of vertical shear to GPI (anomaly), (e) contribution of potential intensity to GPI (anomaly), and (f) contribution of relative humidity to GPI (anomaly). The digits represent the months of the individual cyclogenesis (October is indicated by "0" for brevity). Solid line indicates the meridional phase speed of 4.4° per phase. Dashed line indicates the latitude of 20°N on which cyclogenesis is projected parallel to the solid line in the latitude-adjusted phase analysis in Fig. 12.

disturbance on its northern side based on the composite analysis. Yokoi and Takayabu (2010) showed that a cold surge in the eastern coastal area of the Eurasian continent in April triggered the genesis of Cyclone Nargis in 2008. Frank and Roundy (2006) showed that the tropical cyclogenesis over the NIO seems to be related to some tropical waves. On the other hand, instabilities of the environmental field could develop a finite-amplitude disturbance from an infinitesimal noise. Barotropic instability mentioned above is one of the candidates of such environmental instability. Sufficiently high GPI may also be an environmental instability in which cyclogenesis occurs spontaneously without a preexisting disturbance (Emanuel and Nolan 2004; Nolan et al. 2007). Further case studies are necessary to obtain a comprehensive understanding about the cyclogenesis seeds.

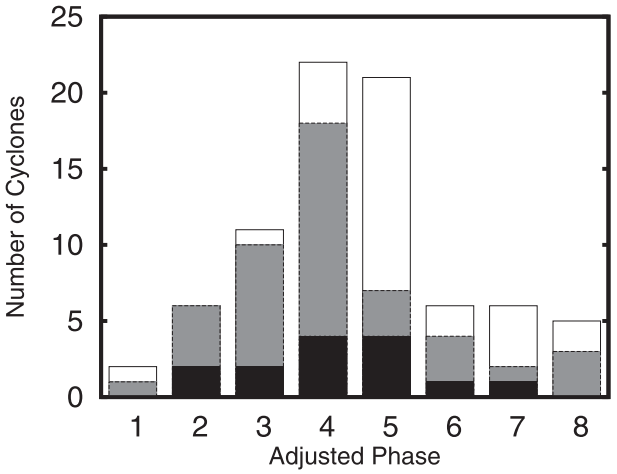

FIG. 12. Numbers of the tropical cyclogenesis in the latitude-adjusted phase of the BSISO. Black, gray, and white bars indicate the numbers in May, June–September, and October, respectively.

7. Summary

The environmental field responsible for tropical cyclogenesis over the BoB is examined using the TC best-track data and atmosphere–ocean analysis data. The GPI index and its four factors (Emanuel and Nolan 2004) are applied to the seasonal and intraseasonal environmental modulations. In the climatological field, the bimodal annual distributions of cyclogenesis and high GPI (Figs. 4a and 13a) are unique to the Bay of Bengal and the Arabian Sea in the north Indian Ocean, which is consistent with previous works (Camargo et al. 2007; Kikuchi and Wang 2010; Evan and Camargo 2011). This is attributed to the weak vertical shear during the premonsoon (~May) and postmonsoon (approximately October–November) over the NIO.

The TC-based composite analysis clarified that a northward-moving signal of high GPI with approximately 30–40-day periodicity is the dominant environmental modulation responsible for the cyclogenesis. The structure of the signal is consistent with the BSISO, which is also unique to the NIO in summer season. Thus, the TC-based composite analysis is useful to identify the dominant environmental modulation of time scales shorter than the seasonal transition. It is interesting to investigate the relation between cyclogenesis and environmental modulation over the other oceans, focusing on the MJO (Camargo et al. 2009) and other intraseasonal dynamics.

The BSISO-based composite analysis showed that the cyclogenesis is active within the high GPI phase of the

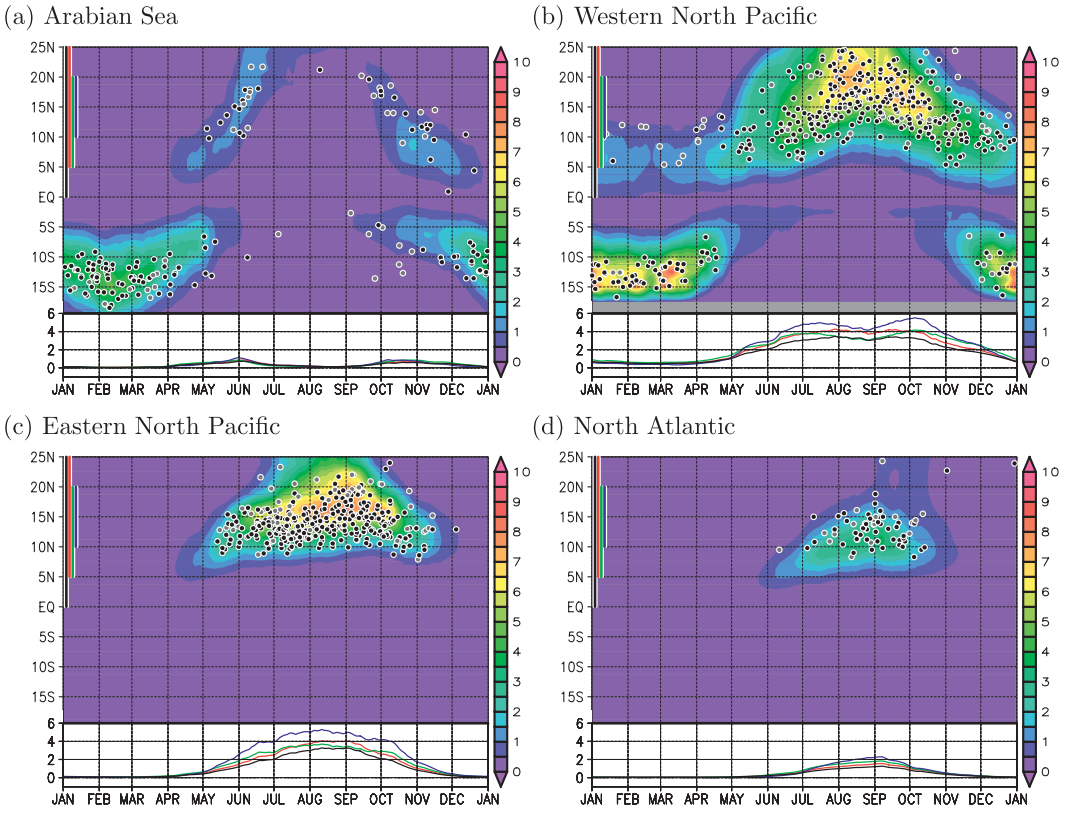

FIG. 13. As in Fig. 4a, but for (a) the Arabian Sea, (b) the western North Pacific, (c) the eastern North Pacific, and (d) the North Atlantic.

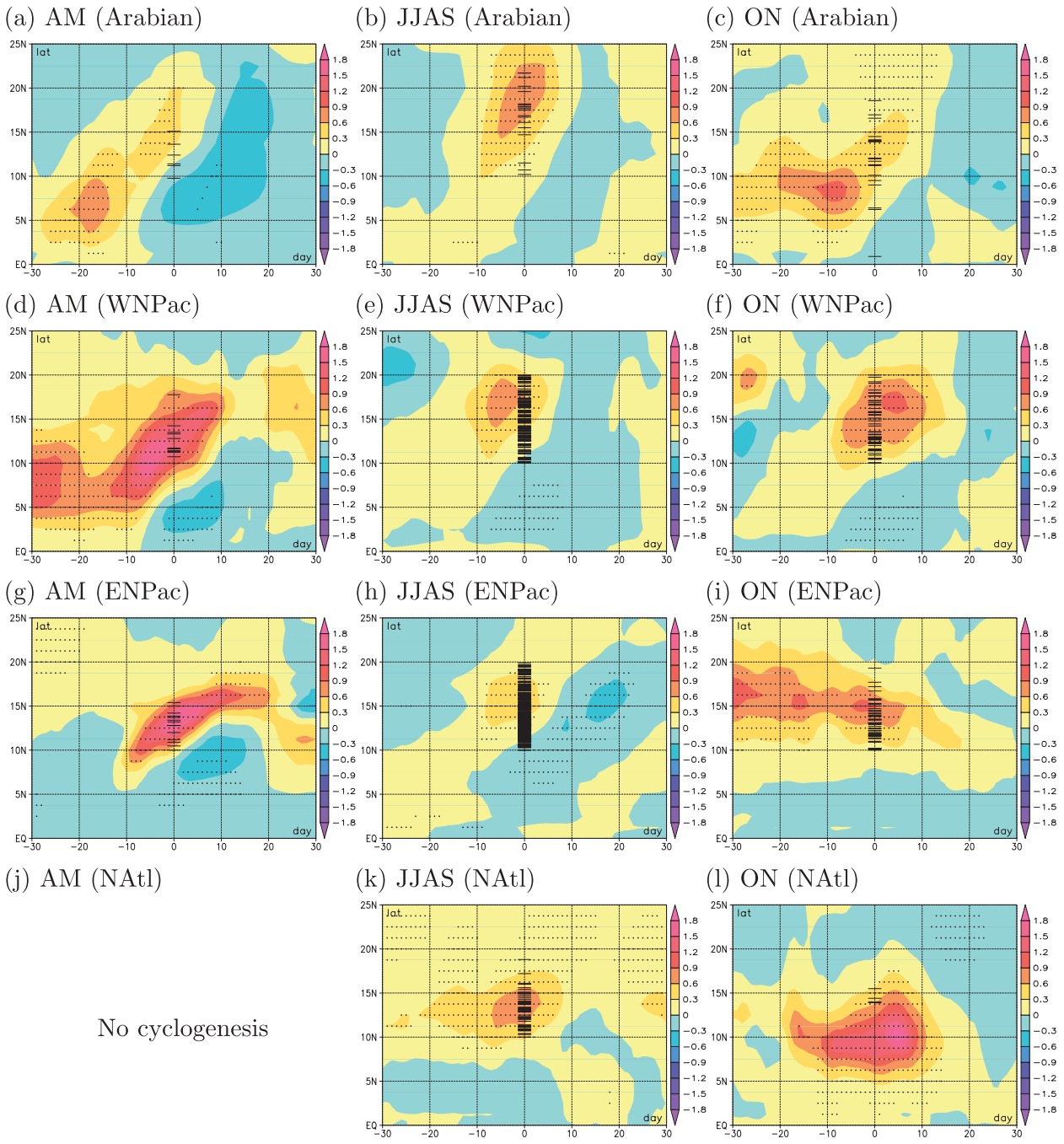

FIG. 14. Time–latitude diagram of the anomalous GPI field over the BoB in the TC-based composite analysis. Diagrams for months of (left) AM, (middle) JJAS, and (right) ON. (a)–(c) The Arabian Sea, (d)–(f) the western North Pacific, (g)–(i) the eastern North Pacific, and (j)–(l) the North Atlantic. The dots and short horizontal bars are as described in Fig. 5.

BSISO, which is consistent with Kikuchi and Wang (2010). We have extended this result to identify the main environmental factors that modulate the GPI within the BSISO. It is revealed that the high GPI phase is attributed to the high relative humidity and large absolute vorticity within the convective phase of the BSISO in all the analyzed seasons. The dominant influence of the relative humidity on the high GPI observed in the BSISO is similar to the characteristics of the MJO described by Camargo et al. (2009). In the mature monsoon, when the vertical shear is climatologically strong, the BSISO also increases GPI by reducing the vertical shear. These

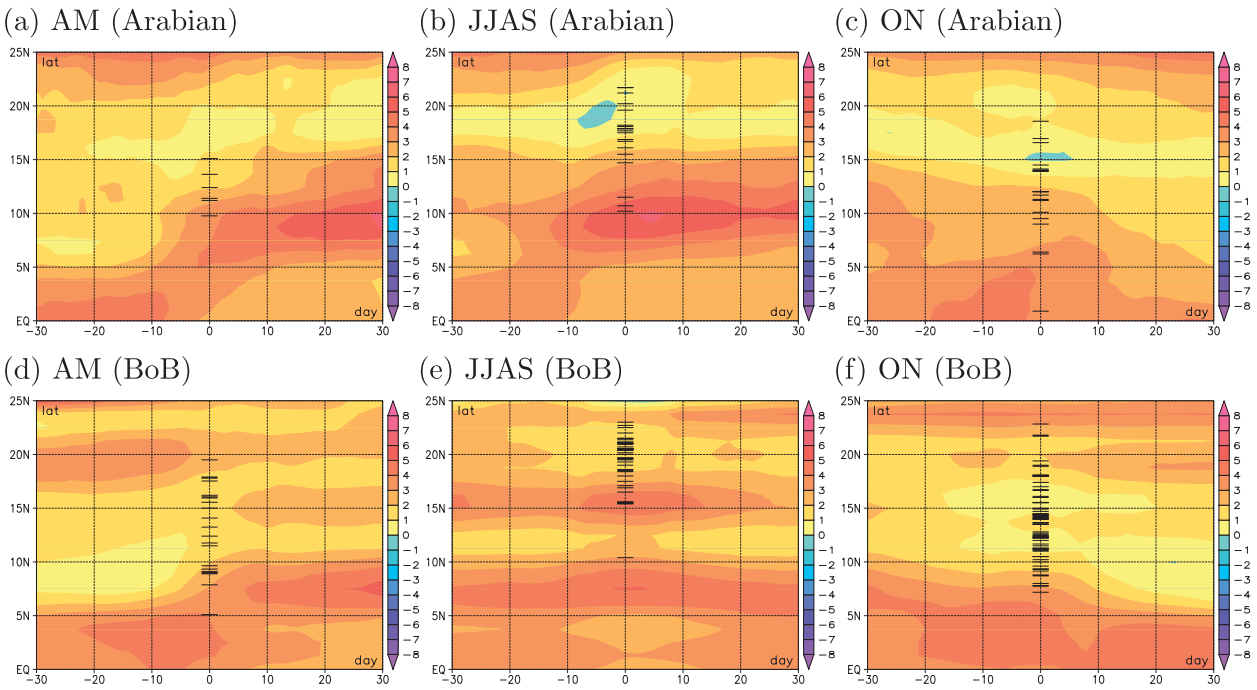

FIG. 15. Time–latitude diagram of the total MGAV field (10^{-11} m^{-1} s^{-1}) in the TC-based composite. Diagrams for months of (left) AM, (middle) JJAS, and (right) ON. (a)–(c) The Arabian Sea and (d)–(f) the BoB. The short horizontal bars are as described in Fig. 5.

results propose that the combination of seasonal and intraseasonal effects is important for the tropical cyclogenesis, rather than the independent effects.

Acknowledgments. We acknowledge helpful comments by Dr. Tetsuo Nakazawa, Dr. Yukari Takayabu, Dr. Satoru Yokoi, Dr. Amato T. Evan, Dr. Suzana J. Camargo, and three anonymous reviewers. The best-track data was obtained from the IBTrACS website. The atmosphere and ocean datasets made use of JRA-25/JCDAS reanalysis, NOAA OI-SST reanalysis, and NOAA OLR data. Potential intensity was calculated using the FORTRAN program from the website of Dr. Kerry Emanuel. This research was supported by Core Research for Evolutional Science and Technology, Japan Science and Technology Agency (CREST, JST), and Grants-in-Aid for Scientific Research 20740266 and 23740349.

REFERENCES

Bister, M., and K. A. Emanuel, 2002: Low frequency variability of tropical cyclone potential intensity 1. Interannual to interdecadal variability. *J. Geophys. Res.,* **107,** 4801, doi:10.1029/2001JD000776.

Camargo, S. J., K. A. Emanuel, and A. H. Sobel, 2007: Use of a genesis potential index to diagnose ENSO effects on tropical cyclone genesis. *J. Climate,* **20,** 4819–4834.

——, M. C. Wheeler, and A. H. Sobel, 2009: Diagnosis of the MJO modulation of tropical cyclogenesis using an empirical index. *J. Atmos. Sci.,* **66,** 3061–3074.

Emanuel, K. A., and D. S. Nolan, 2004: Tropical cyclone activity and global climate. *Proc. 26th Conf. on Hurricanes and Tropical Meteorology,* Miami, FL, Amer. Meteor. Soc., 240–241.

Evan, A. T., and S. J. Camargo, 2011: A climatology of Arabian Sea cyclonic storms. *J. Climate,* **24,** 140–158.

Frank, W. M., and P. E. Roundy, 2006: The role of tropical waves in tropical cyclogenesis. *Mon. Wea. Rev.,* **134,** 2397–2417.

Fritz, H. M., C. D. Blount, S. Thwin, M. K. Thu, and N. Chan, 2009: Cyclone Nargis storm surge in Myanmar. *Nat. Geosci.,* **2,** 448–449, doi:10.1038/ngeo558.

Goswami, B. N., and R. S. A. Mohan, 2001: Intraseasonal oscillations and interannual variability of Indian summer monsoon. *J. Climate,* **14,** 1180–1198.

——, R. S. Ajayamohan, P. K. Xaviers, and D. Sengupta, 2003: Clustering of synoptic activity by Indian summer monsoon intraseasonal oscillations. *Geophys. Res. Lett.,* **30,** 1431, doi:10.1029/2002GL016734.

Gray, W. M., 1975: Tropical cyclone genesis. Colorado State University, Department of Atmospheric Science Paper 234, 121 pp.

Jiang, X., T. Li, and B. Wang, 2004: Structures and mechanisms of the northward propagating boreal summer intraseasonal oscillation. *J. Climate,* **17,** 1022–1039.

Kikuchi, K., and B. Wang, 2010: Formation of Nargis (2008) and tropical cyclones in the northern Indian Ocean associated with with tropical intraseasonal oscillation. *J. Meteor. Soc. Japan,* **88,** 475–496.

Knapp, K. R., M. C. Kruk, D. H. Levinson, H. J. Diamond, and C. J. Neumann, 2010: The International Best Track Archive for Climate Stewardship (IBTrACS) unifying tropical cyclone data. *Bull. Amer. Meteor. Soc.,* **91,** 363–376.

Krishnamurthy, V., and R. S. Ajayamohan, 2010: Composite structure of monsoon low pressure systems and its relation to Indian rainfall. *J. Climate,* **23,** 4285–4305.

Krishnamurti, T. N., P. Ardanuy, Y. Ramanathan, and R. Pasch, 1981: On the onset vortex of the summer monsoon. *Mon. Wea. Rev.,* **109,** 344–363.

Kurihara, Y., M. A. Bender, and R. J. Ross, 1993: An initialization scheme of hurricane models by vortex specification. *Mon. Wea. Rev.,* **121,** 2030–2045.

Madden, R. A., and P. R. Julian, 1972: Description of global circulation cells in the tropics with a 40–45 day period. *J. Atmos. Sci.,* **29,** 1109–1123.

Mao, J., and G. Wu, 2007: Interannual variability in the onset of the summer monsoon over the eastern Bay of Bengal. *Theor. Appl. Climatol.,* **89,** 155–170.

Murakami, T., and T. Nakazawa, 1985: Tropical 45 day oscillations during the 1979 Northern Hemisphere summer. *J. Atmos. Sci.,* **42,** 1107–1122.

——, ——, and J. He, 1984: On the 40–50 day oscillations during the 1979 Northern Hemisphere summer. Part I: Phase propagation. *J. Meteor. Soc. Japan,* **62,** 440–468.

Nolan, D. S., E. D. Rappin, and K. A. Emanuel, 2007: Tropical cyclogenesis sensitivity to environmental parameters in radiative–convective equilibrium. *Quart. J. Roy. Meteor. Soc.,* **133,** 2085–2107.

Onogi, K. J., and Coauthors, 2007: The JRA-25 Reanalysis. *J. Meteor. Soc. Japan,* **85,** 369–432.

Reynolds, R. W., N. A. Rayner, T. M. Smith, D. C. Stokes, and W. Wang, 2002: An improved in situ and satellite SST analysis for climate. *J. Climate,* **15,** 1609–1625.

Rotunno, R., and K. A. Emanuel, 1987: An air–sea interaction theory for tropical cyclones. Part II: Evolutionary study using a nonhydrostatic axisymmetric numerical model. *J. Atmos. Sci.,* **44,** 542–561.

Webster, P. J., 2008: Myanmar's deadly daffodil. *Nat. Geosci.,* **1,** 488–490.

Yanase, W., H. Taniguchi, and M. Satoh, 2010: The genesis of tropical cyclone Nargis (2008): Environmental modulation and numerical predictability. *J. Meteor. Soc. Japan,* **88,** 497–519.

Yasunari, T., 1981: Structure of an Indian summer monsoon system with around 40-day period. *J. Meteor. Soc. Japan,* **59,** 336–354.

Yokoi, S., and Y. Takayabu, 2010: Environmental and external factors of tropical cyclone Nargis in April 2008 over the Bay of Bengal. *J. Meteor. Soc. Japan,* **88,** 425–435.